PAPER

www.rsc.org/loc

Design of microfluidic channel geometries for the control of droplet volume, chemical concentration, and sorting†

Yung-Chieh Tan,[a] Jeffrey S. Fisher,[a] Alan I. Lee,[a] Vittorio Cristini[ab] and Abraham Phillip Lee*[ac]

[a] *Department of Biomedical Engineering, 204 Rockwell Engineering Center, Irvine, CA. 92697, USA. E-mail: aplee@uci.edu. E-mail: ytan@uci.edu. E-mail: cristini@math.uci.edu*

[b] *Department of Mathematics, 204 Rockwell Engineering Center, Irvine, CA. 92697, USA*

[c] *Department of Mechanical Engineering, 204 Rockwell Engineering Center, Irvine, CA. 92697, USA*

Received 2nd March 2004, Accepted 3rd June 2004
First published as an Advance Article on the web 1st July 2004

Passive microfluidic channel geometries for control of droplet fission, fusion and sorting are designed, fabricated, and tested. In droplet fission, the inlet width of the bifurcating junction is used to control the range of breakable droplet sizes and the relative resistances of the daughter channels were used to control the volume of the daughter droplets. Droplet fission is shown to produce concentration differences in the daughter droplets generated from a primary drop with an incompletely mixed chemical gradient, and for droplets in each of the bifurcated channels, droplets were found to be monodispersed with a less than 2% variation in size. Droplet fusion is demonstrated using a flow rectifying design that can fuse multiple droplets of same or different sizes generated at various frequencies. Droplet sorting is achieved using a bifurcating flow design that allows droplets to be separated base on their sizes by controlling the widths of the daughter channels. Using this sorting design, submicron satellite droplets are separated from the larger droplets.

Introduction

Droplets in microfluidic systems are promising biological and chemical picoliter reactors as the reaction time and chemical concentration in each droplet can be precisely controlled. Many advantages of using droplets have recently been reported. One such advantage is the rapid mixing of liquids that are normally hindered in low Reynolds number single phase laminar flow.[1–5] Droplet based microfluidic devices have shown great promise for lab on chip applications. Zheng *et al.*[6] have demonstrated protein screening in droplets using parallel stream flows, and Hirano *et al.*[7] have obtained successful crystal growth in mixed droplets. Real time polymerase chain reaction in droplets has been demonstrated by Pollack *et al.*,[8] and electrophoresis using a droplet based handling system has been demonstrated by Kaneda and Fujii.[9] Burns *et al*. integrated a droplet dispensing system into a DNA analyzer,[10] Srinivasan *et al*. constructed a droplet based system that can analyze human physiological fluids,[11] and Schaack *et al*. demonstrated cell growth in microdrops.[12]

The versatility of droplet microfluidic systems lies essentially in the ability to transport and precisely "dial-in" fluid volumes of each individual droplet. This can be achieved either actively or passively. Active control generates local forces to direct droplet movements and allows each droplet to be individually manipulated in desired path ways.[13] This can be achieved using electrowetting,[5,8,11,14–19] dielectrophoresis,[20,21] electrostatic,[7,22] pneumatic pressure,[3] and thermocapillary[23] actuation. Passive control uses externally generated flows that are varied locally either by the geometry of the channels[4,6,24,25,27–31] or by surface wetting patterns[26] to manipulate droplets. Most passive devices are focused on the generation of droplets from continuous streams.[27–31] Since flow is controlled by the geometry, the flexibility to reconfigure droplets is limited. However, this is compensated by the high efficiency of droplet generation. The speed of droplet generation from a nanojet microfluidic droplet generation system ranging from 100 ms drop^{-1} to <0.2 ms drop^{-1} were reported[27] and thus provides a very efficient means to sample combinations of mixing conditions.[4,6,24,25] Furthermore, since droplets are suspended in another liquid medium, and the sizes are controlled by the relative flow rates, problems associated with active system such as solvent evaporation in air drops,[24,32,33] absorption of bio-molecules to the wetting surface,[19] minimum pitch size used to control tiny droplets,[18] and maximum actuation voltage required to move large droplets are avoided.[22]

We have developed various new microfluidic designs to enhance the control of droplets in the channels, primarily focusing on the geometry of bifurcation junction. Techniques for droplet fission[34,35] and fusion[4] allows fluid volume in each droplet to be reduced or increased, while sorting allows droplets to be filtered and separated by size. Although aspects of critical break-up condition for symmetric fission in channels with square cross sections have been detailed by Link *et al.*,[35] here we investigate the applicability of the break-up criteria to channels with rectangular cross sections. For asymmetric fission we extend previous studies of Song *et al.*[4] and Link *et al.*[35] on the dependence of droplet volumes to channel resistances. In addition, to the best of our knowledge, we demonstrate here for the first time (1) the use of droplet fission to control the concentration of chemicals inside droplets, (2) sorting of droplets based on flow patterns at bifurcation junctions, (3) the generation and collection of nano sized satellite droplets, and (4) droplet fusion using the flow rectifying design to coalesce two or more droplets regardless of size. Previous studies on droplet fusion by Song *et al*.[4] was limited to droplets of difference sizes.

Materials and methods

Droplets are generated using nanojet design[27] to allow the control of droplet size and generation rate. The microfluidic channel is made of PDMS molded imprints bonded to a microscopic glass slide.[36] No active pressure control or valving are required to manipulate droplets. Pure oleic acid (Fisher Sci.) and water are used as the continuous and dispersed phase, and both solutions are injected using syringe pumps (pico plus from Harvard Apparatus). The process of droplet fission, sorting, and fusion are recorded with fast speed cameras.

† Lab on a Chip special issue: *The Science and Application of Droplets in Microfluidic Devices*.

DOI: 10.1039/b403280m

Results and discussion

Control of droplet fission

Droplet break-up events can be used to reduce the size of generated droplets. For droplets generated with chemical gradients,[4] the reaction time and chemical concentration in each of the daughter droplets depend on the fission mechanism.

The mechanism for droplet break-up in immiscible shearing flows has been thoroughly investigated.[37–41] Essentially, droplet break-up occurs when the viscous stress exerted by the continuous phase induces a critical asymmetric stress on the droplet causing an imbalance of the surfacing tension.[37] This is generally described by the capillary number, here defined as $Ca = \eta v/\gamma$,[35] where η is the viscosity of the oil phase, v is the velocity of the droplet entering the junction, and γ is the interfacial tension between water and oil. When Ca is greater than the critical capillary number (C_{cr}), droplet fission occurs. Since C_{cr} depends on the type of shear strain exerted by the flow, C_{cr} required to produce droplet fission can be varied accordingly by changing the input flow rates of the mother channel Q_0 and the output flow rates of the two daughter channels (Q_1 and Q_2) as shown in Fig. 1. Since the droplet moves at about the same velocity as the continuous oil phase, v of droplet is equal to the ratio of the applied oil flow rate to the cross sectional area. Previous studies on symmetric break-up conditions by Link *et al.*[35] showed that the critical capillary number varies according to $C_{cr} = \alpha\varepsilon_0(1/\varepsilon_0^{2/3} - 1)^2$, where α is a dimensionless constant equal to 1 for square channels, and ε_0 is the initial extension ratio which expressed using variables from Fig. 1 is $L_d/\pi W_i$.

When the flow is fully symmetric, the forces exerted on the two halves of the mother droplet are equal, and if the droplet is not breakable by the flow, the droplets are randomly distributed into the daughter channels. In the case when the droplet is breakable by flow, droplet fission creates two equal sized daughter droplets as shown in the insert of Fig. 2. The three inlet dimensions studied here all have channel heights, h, equal to 40 μm, and consist of one square channel cross section and two rectangular channel cross sections with widths W_i equal to 70 μm and 100 μm, respectively. In comparing the square and rectangular channel, the equivalent width of a square with same cross section is used to determine the extension ratio for rectangular channels. The results are shown in Fig. 2. For square channel the criteria for droplet break-up agrees strongly with Link *et al*.[35] For channels with different geometries, C_{cr} with $\alpha = 1$ does not predict droplet break-up. In general we found that when the height of the channel is constant, the range of breakable droplet sizes decreases with increasing inlet channel width as indicated by the observed smallest droplet breaking diameter shown in Table 1. Under a constant Q_o, decreasing the inlet width of the channel increases the shear stress exerted on the droplet. As a result when the width of the mother channel is narrow, smaller minimum break-up diameter is observed.

Under asymmetric flow, the streamlines divide according to the flow rates inside the daughter channels. When a droplet traveling along the center of the channel, reaches the bifurcating junction, the pressure and shear forces that pull the droplet into each daughter channel are proportional to the droplet surface area exposed to those stream lines. If the forces are larger than the surface tension of the droplet, it splits into two drops of unequal sizes.

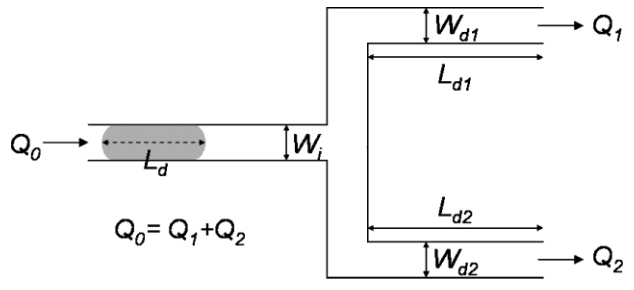

Fig. 1 Schematic of the bifurcating junction. Droplet with length L_d inside the mother channel moves toward the bifurcating junction connecting the two daughter channels.

In designing the asymmetric junction, the inlet width and the height of the channel are minimized to be 40 μm to allow the widest range of breakable droplet sizes. The width difference of the daughter channels are used to vary the bifurcating flow. By controlling the respective width ratio (W_{d1}/W_{d2}) to be 30 μm/60 μm, 30 μm/90 μm, and 30 μm/120 μm, the flow bifurcates according to the following (Q_1/Q_2) ratios: 1/1.8, 1/2.1, and 1/2.2

The range of minimum breakable droplet size for asymmetric flow is presented in Table 2 as a set of extensional numbers with an upper limit of ε_u, for droplets that break and a lower limit of ε_l, for droplets that don't break. The upper and lower limits of these extensional numbers would show up in the lower right corner of Fig. 2 indicating that the break-up under these asymmetric conditions occur at a much higher extensional number than under symmetric break-up conditions. This agrees with qualitative observation of Link *et al.*,[35] and is consistent with other previous studies, which showed that critical capillary number increases as flow becomes more asymmetric.[37–40]

Since the lengths of a droplet in channel is directly proportional to its volume, the volume ratio of the daughter drops under asymmetric fission can be determined by the length ratio of the two daughter drops. Previous observations by Song *et al.* and Link *et al.*, suggested that daughter droplet volume is inversely proportional to the resistance of the channels. Our data suggested that daughter droplet volume depends on both the channel resistances

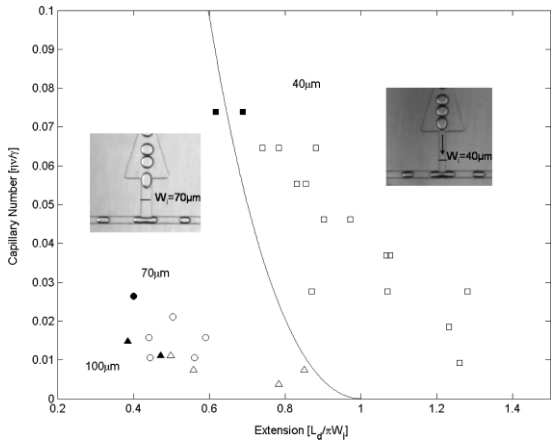

Fig. 2 Channels with different inlet cross sections have different critical break-up criteria. Clear marks indicate breaking drops while filled marks indicate non-breaking drops. The squares, circles, and triangles indicate channels with inlet width of 40 μm, 70 μm, and 100 μm respectively. The break-up criteria for square cross sectional area agrees with Link *et al.*,[35] such that critical condition varies according to $C_{cr} = \varepsilon_0(1/\varepsilon_0^{2/3} - 1)^2$ as shown by the solid line.

Table 1 Effect of channel width (W_i) on minimum breaking diameter (D)

W_i/μm	D/μm	Ca
40	43	0.065
70	69	0.021
100	92	0.011

Table 2 Ranges of minimum droplet sizes under asymmetric break-up conditions

W_d:30μm	ε_u[a] | Ca	ε_l[b] | Ca
60	1.45 | 0.0156	1.31 | 0.0208
90	2.85 | 0.0104	1.78 | 0.0104
120	2.71 | 0.0104	1.57 | 0.0104

[a] ε_u: minimum extensional number for a breaking drop [b] ε_l: maximum extensional number for a none-breaking drop

and the volume of the mother drop. In Fig. 3, the ratios of larger-to-smaller daughter droplets (L_S/L_D) after asymmetric fission indicated that the ratio of daughter droplet volumes changes with the size of the mother drop. If the ratio is independent of the sizes of the mother droplets, then the smaller daughter droplet in the bottom photo of Fig. 3 would be smaller than the corresponding daughter droplet in the upper photo. While we did not specifically verify the droplet volume ratio that is equivalent to the ratio of channel resistances,[35] it appears from Fig. 3 that ratio decreases with decreases in mother droplet size, which suggests that the daughter volume ratio identical to ratio of bifurcating flow is achievable for smaller droplet sizes.

For many biological assays, it is desirable to rapidly sort biological samples into various volumes and concentrations for analytical and combinatorial purposes. This is often difficult and cumbersome with current electrode-based droplet platforms, as it would require programmed synchronization of many electrodes to process a single stream of droplets[13] In the droplet fission system presented here, a single bifurcating junction can create two organized streams of droplets with sizes controlled by the design of the bifurcating flow. With multiple bifurcating junctions, parallel streams of controlled liquid volume in droplets can be rapidly analyzed. Droplets with diameters approaching ~ 1 μm or less, can also be generated during near critical break-up conditions. These droplets are generated through multiple asymmetric fission junctions using the channel shown in Fig. 4.

Control of chemical concentration in daughter droplets

When chemicals of various concentrations are generated inside the droplet, fission of the droplet allows chemical mixing to be further quantified. The reagents are allowed to mix until reaching the bifurcating junction. By controlling the type of bifurcating flow and the location of droplet fission, the chemical concentration and reaction time inside each daughter droplet can be controlled. The fission system shown in Fig. 4 divides the flow according to 26.25%:73.75%, 21.96%:52.06%, and 22.50%:29.56% of the total flow.

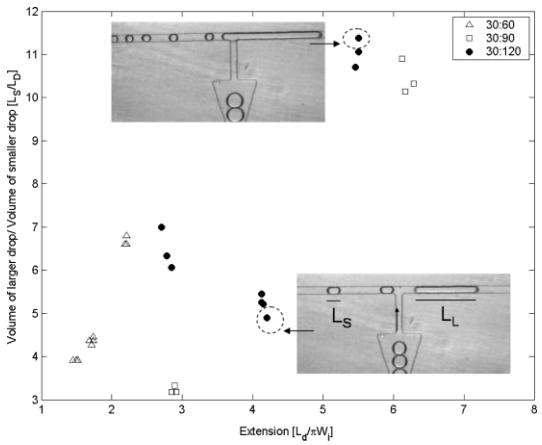

Fig. 3 Volume ratio of the daughter droplets (L_S/L_D) changes according to the size of the mother droplet. The breaking of the drops are shown in the photos.

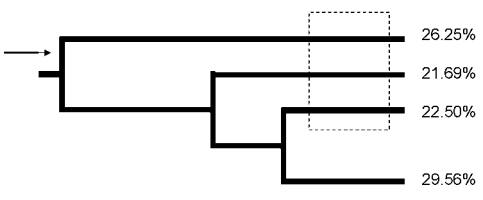

Fig. 4 Schematic of channel with multiple bifurcating junctions used to control the final concentration of chemical mixing. The box indicates the region observed under microscope.

To verify that fission of droplets can be used to control chemical concentration of each daughter droplet, dye solution containing 5% w/v of naphthol blue black (Fisher Sci.) in DI water was mixed inside a droplet with water at a 1:2 ratio. After fission, the concentration of dyes in daughter droplets were calculated as a percentage of the original dye solution.

Since the bifurcating point is located right after droplet generation, the droplet splits before mixing is completed, as a result the dye concentrations in the final daughter droplets are determined by the mixing pattern of droplet at the bifurcating junction. All daughter droplets contained dye concentration in between the range of pure dye (100%) and full mixing (33%) of the pure dye with water as shown in Fig. 5. The sizes of daughter drops in each channel are monodispersed with a size variation of $< 2\%$. Since each emulsion can be considered as a unique reaction vessel capable of containing the same reaction conditions for a population study or different reaction conditions for a variable study, the uniform droplet size distributions would reduce uncertainties associated with volume variations.

Control of droplet circulation

In the microcirculation of the body, controlling red blood cell (RBC) concentration by volume flow is critical for the delivery of oxygen to tissues. Analogously, the control of droplet circulation is important for transporting reagents in droplets.

The simplest geometry to control droplet flow is the asymetric bifurcating junction shown in Fig. 6. The flow rates of the daughter channels are controlled to be identical, and due to the difference in local widths of the daughter channels, the higher fluid velocity created by shorter channel width induces a greater shear stress on the droplet, moving it toward the daughter channel.[42] By the same token, when a droplet is large enough to plug the inlet channel, the pressure force drives the droplet toward the channel with the smaller width.[42] In both cases, the forces driving the object is dependent on the area projected by the flow and the width ratio of the daughter channels.[42] In our sorting device, we have observed that the majority of droplets centered toward the middle of the bifurcation junction are always driven toward the daughter channel with smaller inlet width.

In the initial sorting design, the pure water in oil system generated droplets that fuse at the expansion, which accumulated into a plug in the daughter channel that affected droplet sorting. To

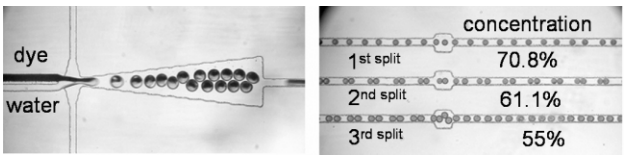

Fig. 5 Control of concentration in droplets by fission mechanism. Droplets are generated with a dye to water volume ratio of 1:2 inside the droplet (left). After the mother droplet breaks in succession at the three bifurcating points, each stream of daughter droplets contained different final fractions of the original dye concentration (right).

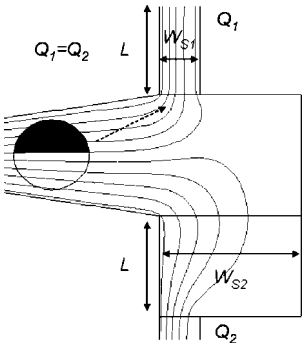

Fig. 6 Due to the local velocity difference between the daughter channels, a droplet moves toward the channel with shorter width.

reduce droplet coalescence, span 80 surfactant was added into the oil phase, which generated separation pattern shown in 7. The sorting efficiency in this design is limited by both the droplet size and the rate of droplets going through the daughter channels. When a large droplet plugs the smaller daughter channel, the sorting of the next successive drop will be hindered, causing it to flow into the other daughter channel as observed in the case of an incomplete sorting shown in Fig. 7b.

Subsequent tests with 15 μm microbeads did not result in sorting patterns. While, the relationship between droplet size, generation speed, surface stiffness and flow is not fully determined in this paper, it will be characterized in future studies. Here we want to focus on solving the issue of droplet coalescence in the sorting channel to allow surfactant free droplets to be sorted and later fused in a controllable fashion.

To reduce droplet coalescences, a loop channel shown in Fig. 8 is used to replace the width expansion. The looping region reduces the dead volumes required to sort droplets, which prevents droplet accumulations. In this new design, incomplete sorting was not observed, and the generated droplet either sorts or splits as shown in Fig. 8. The sorting of surfactant free droplet is important for droplet based assays, such that it allows droplet volume to be modified by fission and fusion, and the sensitive droplet contents are not affected by surfactant chemicals.

For the case of small droplets, in which the droplet lies entirely away from the dividing stream interface the droplet will not be sorted by the width difference at the junction, but will instead be carried by one of the bifurcating flow into the respective daughter channel as shown in Fig. 9a. This is consistent with experimentally observed distribution of 15 μm beads that are randomly distributed into both daughter channels. There is therefore a minimum sorting dependency on droplet area projected by the flow. Similarly, sorting based on droplet sizes can be realized through controlling both the flow rate and the width of each daughter channel. An example is shown in Fig. 9b: while both droplets are flowing in the middle of the channel, the larger droplet is exposed to streams flowing toward both daughter channels, but the smaller droplet is being carried by only the stream flowing toward the bottom channel. Due to the higher net force created by the difference in widths of the daughter channels, the larger droplet sorts into the upper channel, and due to the total submersion in the lower stream, the smaller droplet sorts into the bottom channel.

Droplet sorting can be useful for many applications, here we apply the sorting device to separate nano-sized satellite droplets from the main stream.

Satellite droplets are generated along with large monodispersed droplets without using surfactant, and they are sorted using the loop sorting design. The larger primary droplets are separated into the daughter channel with higher flow velocity, while satellite droplets with diameters of ~ 1 μm are carried by the flow into the daughter channel containing the loop structure, and are eventually collected as shown in Fig. 10. Nano-sized droplets are potentially useful in a multitude of applications, such as sensitive sample analysis assays that require rapid mixing inside tiny droplets, drug production processes that involve control of pico to femto liters of reagents, and gene therapies that rely on the successful encapsulation of nano-sized liposomes. Alternatively, this design can serve to filter out satellite droplets in applications where they are undesirable, increasing the degree of monodispersity of the primary droplets.

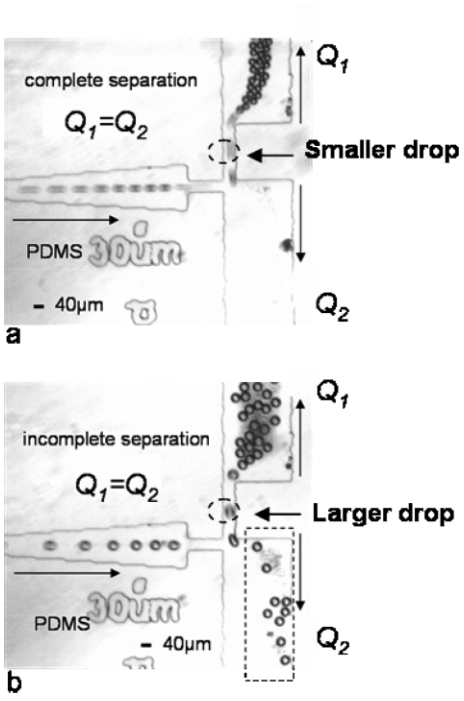

Fig. 7 Sorting of droplets. (a) complete sorting indicates that all droplets moved toward the desired daughter path. (b) The larger droplet size temporarily alters the channel resistance, and thus hindered the sorting of the next successive drop causing incomplete sorting.

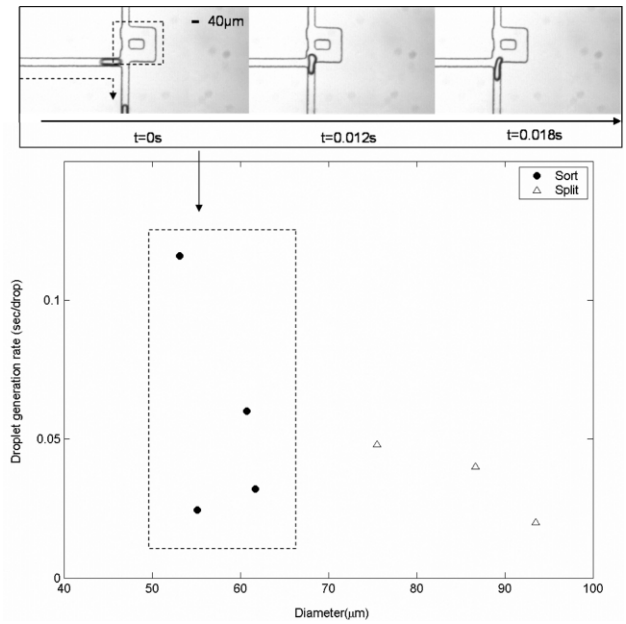

Fig. 8 Sorting of the loop channel design under equal bifurcating flow rates. The loop channel design prevents the coalescence of droplet at the junction allowing surfactant free droplets to be sorted. The plot shows that no incomplete sorting was observed: the droplet either sorts or splits. The photo above shows the droplet motion near the bifurcating junction, where the droplets are sorted into the bottom channel.

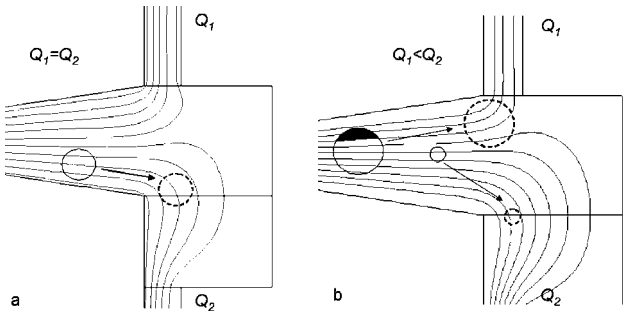

Fig. 9 The size and the location determine the sorting behaviour of the droplet. (a) Droplet fully immersed in the bottom streamlines travels toward the lower channel at the bifurcating junction independent of the velocity difference between the two daughter channels. (b) Droplets that lie between the dividing streams of upper and lower channels experience a net shear stress moving droplet toward the upper channel. Flow rates of the bottom channel can be increased to optimize the maximum sorting of smaller droplets.

Fusion of droplets

To coalesce two or more droplets in the microfludic channels requires the removal of the continuous phase separating them. When two droplets come into close contact, a thin liquid bridge forms between the droplets due to the attractions between molecules. The high curvature meniscus formed around the bridge creates an imbalance of the surface tension that quickly coalesces the two droplets.[43] To form the initial contacts between droplets, fluid between droplets must be removed. This can be achieved through expanding the channel junction as shown in Fig. 11a. The volume fluid between droplets can also be reduced through setting faster droplet generation rate.

We have experimented with the three different channel geometries as shown in Fig. 11 containing either a straight expansion, a tapered expansion, or a flow rectifying design in which droplets are focused and fused in the middle of the junction by balancing the net shear forces. Droplet fusion in the rectangular expansion design works at a limited range of rates and sizes determined by the length and the width of the expansion. The tapered expansion, which is equivalent to a series combination of rectangular ones, works at a wider range of sizes and rates but can allow undesired multiple fusions. Among the three designs, the flow rectifying design provides the most flexibility in fusing droplets as demonstrated in Fig. 12. Simultaneous fusion of three or more droplets have also been observed with this design. The mechanism of this type of fusion qualitatively agrees with mechanism described by Nikolayev *et al.*,[44] in which the fusion of two droplets initiates an internal flow inside the droplet that induces additional coalescence of surrounding droplets.

The flow rectifying design allows the fluid volume between drops to be separated at controllable rates, whereas other designs provide fixed rates based on the width of the expansion. In the flow rectifying design, the separating fluid volume flows into the upper and lower channels at a rate controlled by the resistance of the identical upper and lower channels. This allows equal fluid volume to be removed by the upper and lower channels, but does not generate net force along the vertical axis. By controlling the separating flow rates, the speed at which droplets approach each other at the junction can be tuned to allow desired droplet fusion to occur.

In a more complex system involving fusion of different types of droplets, each type of reactant inside the fused droplet can be arranged in order. An example of such mixing is shown in Fig. 13, in which if the dye droplet enters the junction first, the dye content becomes more concentrated at the head of the fused droplet and *visa versa*.

As demonstrated in an earlier section, droplet fission can be used to control the chemical concentration of each daughter droplets. Since fission is perpendicular to the direction of flow, the chemical concentrations distributed to the daughter droplets are dependent on the chemical gradient of the mother droplet oriented in the direction of flow. The chemical gradient generated using co-flow stream is parallel to the direction of flow, while the chemical gradient generated after droplet fusion in flow rectifying design is perpendicular to the direction of flow. This provides additional freedom to control how the partial concentrations of the chemicals in the original droplet divide among the daughter droplets.

Temporal droplet rearrangement

In the flow rectifying design, fusing droplets from different streams requires that the droplet generation rate of each stream be coordinated at a set frequency to achieve the desired fusion combination. An alternative approach is to rearrange the order of droplets in a single stream. One design of a droplet rearranger consists of a loop with a width larger than the width of the channel, as shown in Fig. 14. Without any droplets present, the straight path

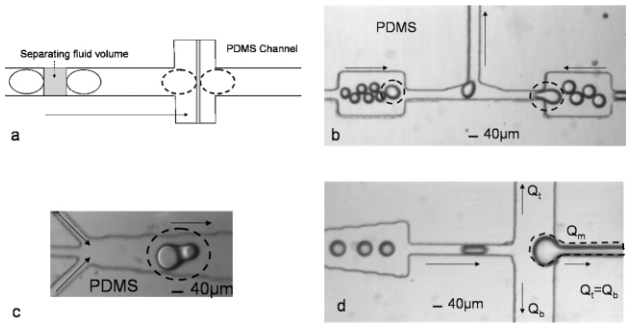

Fig. 11 Methods of droplet fusion. Fused droplets are shown in circles. (a) Principle of droplet fusion. Droplets are allowed to fuse when the distance separating them is shortened. (b) Fusion inside an expanding straight channel. (c) Fusion in channel with tapered expansion. (d) Fusion in flow rectifying design. The larger droplet shown in right is the result of coalescence of several smaller droplets.

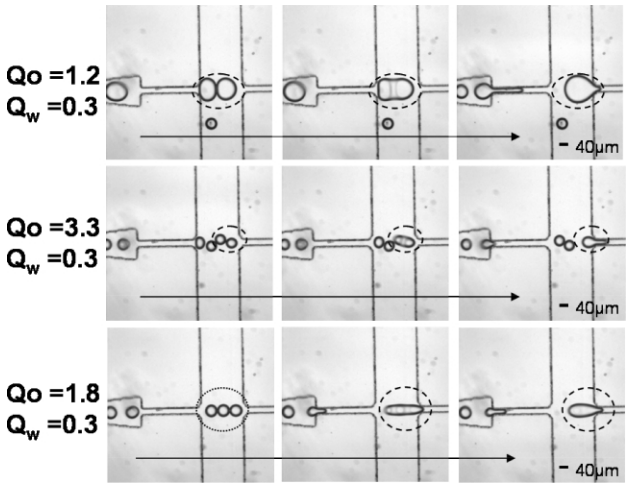

Fig. 12 Flow rectifying design for controlled fusion of droplets. Top, fusion of two large droplets, middle, fusion of two smaller droplets, and bottom fusion of three droplets

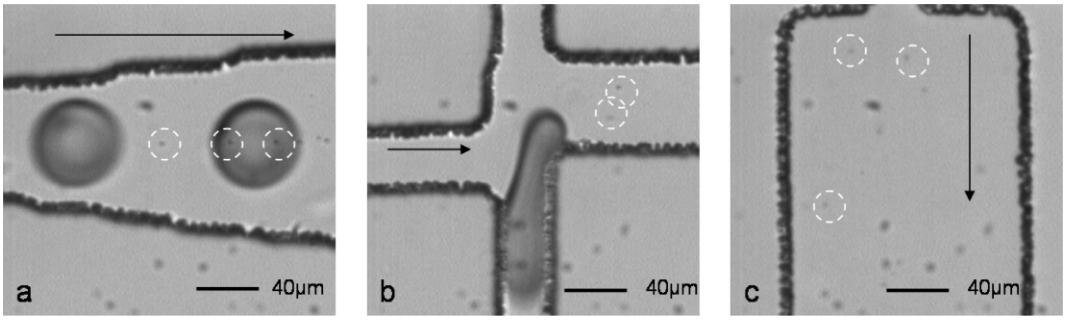

Fig. 10 The creation, sorting and collection of satellite droplets. (a) satellite droplets are created with larger primary droplets. (b) primary droplets are sorted toward the lower daughter channel while satellite droplets are sorted into the loop region. (c) The channel collecting the satellite droplets is free of primary droplets.

possesses the least resistance and highest flow; therefore, an isolated droplet would simply follow the straight path through the device. However, the presence of other droplets can alter the resistance, sending droplets into the loop path. The lower flow rate and longer path distance result in a longer travel time for the droplet in the loop path, causing it to re-enter the droplet series in a different position. Of course, in a series of identical droplets, such a shift has little meaning. But with a droplet series that possesses even a simple, but defined, variability (droplet size, chemical concentration, reagent content, *etc.*) this design can introduce desired organization into the stream. Such a stream with an ordered series of droplets could then proceed through fusion and fission devices for automated and intricate combinatorial assays.

Conclusion

The various methods of droplet control presented here could be built into a single platform or used in combination with other electrode based platforms to achieve control of high-speed droplet fission, fusion, sorting, and rearranging in the microfluidic channel. Since the emulsion vessels are microns in size, the reaction volume can be pico-liter or smaller. A microliter of reagent can generate more than 10^6 reaction vessels. This greatly reduces the amount of reagent that is needed to run each reaction, a feature that is extremely useful for high throughput screening. Additionally, unlike the other current platforms, this device offers ways to control nano-sized satellite droplets. Sorting satellite droplets from the primary drops provides an efficient way for nano-sized droplets to be processed in the microfluidic channel. The efficiency of this system is ideal for generating droplet based products that require fixed steps of processing. Since the channels are fabricated without electrodes, multiple devices can be repeatedly fabricated from a single mold. The simplicity of fabricating these channel designs allows this platform to be used as a disposable system that can be massively produced at low costs.

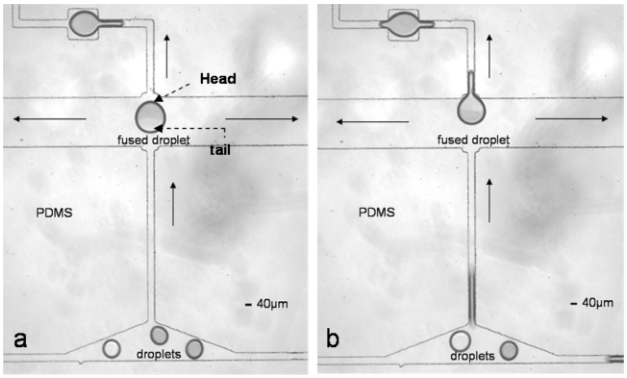

Fig. 13 Mixing of droplets. The created chemical gradient after fusion is perpendicular to the motion of the droplet. Depending on the order of the droplet arrangement, the chemical gradient inside the droplet can be varied as shown in (a) the blue dye concentrates near the head of the droplet, or in (b) the blue dye is concentrated at the tail of the droplet.

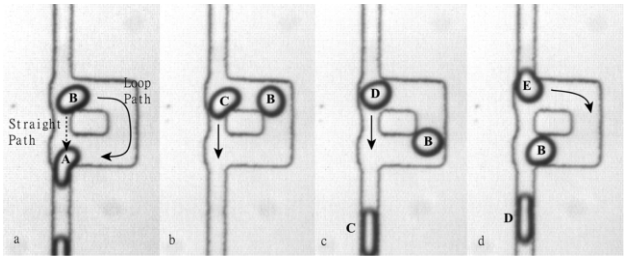

Fig. 14 Droplets are rearranged in a loop channel design. (a) The presence of droplet A at the outlet causes a reaction pressure along the straight path that forces B into the loop path. (b–c) With the outlet open, droplets C and D travel the straight path. (d) B enters the outlet, continuing the cycle by forcing E into the loop path. Droplet B has been shifted to a position after C and D.

Acknowledgements

The authors would like to acknowledge funding from the National Science Foundation and the assistance of Dr John Collins in technical discussions and Eugene Lin in taking measurements.

References

1 K. Handique and M. Burns, *JMEMS*, 2001, **11**, 548.
2 H. Kinoshita, M. Oshima, S. Kaneda, T. Fujii, T. Saga and T. Kobayashi, *7th International Conference on μTAS*, 2003, 535.
3 K. Hosokawa, T. Fuji and I. Endo, *Anal. Chem.*, 1999, **71**, 4781.
4 H. Song, J. D. Tice and R. F. Ismagilov, *Angew. Chem. Int. Ed.*, 2003, **42**(7), 767.
5 P. Paik, V. K. Pamula and R. B. Fair, *Lab Chip*, 2003, **3**, 253.
6 B. Zheng, L. S. Roach and R. F. Ismagilov, *J. Am. Chem. Soc.*, 2003, **125**, 11170.
7 M. Hirano, T. Torii, T. Higuchi, M. Kobayashi and H. Yamazaki, *7th International Conference on μTAS*, 2003, 473.
8 M. G. Pollack, P. Y. Paik, A. D. Shenderov, V. K. Pamula, F. S. Dietrich and R. B. Fair, *7th International Conference on μTAS*, 2003, 619.
9 S. Kaneda and T. Fujii, *7th International Conference on μTAS*, 2003, 1279.
10 M. A. Burns, B. N. Johnson, S. N. Brahmasandra, K. Handique, J. R. Webster, M. Krishnan, T. S. Sammarco, P. M. Man, D. Jones, D. Heldsinger, C. H. Mastrangelo and D. T. Burke, *Science*, 1998, **282**, 484.
11 V. Srinivasan, V. K. Pamula, M. G. Pollack and R. B. Fair, *7th International Conference on μTAS*, 2003, 1287.
12 B. Schaack, B. Fouque, S. Porte, S. Combe, A. Hennico, O. Filholcochet, J. Reboud, M. Balakirev and F. Chatelain, *7th International Conference on μTAS*, 2003, 669.
13 K. F. Böhringer, *7th International Conference on μTAS*, 2003, 591.
14 M. G. Pollack, A. D. Shenderov and R. B. Fair, *Lab Chip*, 2002, **2**, 96.
15 M. G. Pollack, R. B. Fair and A. D. Shenderov, *Appl. Phys. Letter.*, 2000, **77**(11), 1725.
16 J. Lee, H. Moon, J. Fowler, T. Schoellhammer and C. J. Kim, *Sens. Actuators, A*, 2002, **95**, 259.
17 S. K. Cho, H. Moon and C. J. Kim, *JMEMS*, 2003, **12**(1), 70.
18 H. Ren, V. Srinivasan, M. Pollack and R. B. Fair, *7th International Conference on μTAS*, 2003, 993.
19 J. Y. Yoon and R. L. Garrell, *Anal. Chem.*, 2003, **75**, 5097.
20 J. A. Schwartz, J. V. Vykoukal and P. R. C. Gascoyne, *Lab Chip*, 2004, **4**, 11.
21 T. B. Jones, M. Gunji, M. Washizu and M. J. Feldman, *J Appl. Phys.*, 2001, **89**(2), 1441.
22 T. Taniguchi, T. Torii and T. Higuchi, *Lab Chip*, 2002, **2**, 19.
23 A. A. Taniguchi, J. P. Valentino, S. M. Troian and S. Wagner, *JMEMS*, 2003, **12**(6), 873.
24 M. Spaid, A. Chow and Y. Yurkovetsky, *7th International Conference on μTAS*, 2003, 445.
25 J. S. Go, E. H. Jeong, K. C. Kim, S. Y. Yoon and S. Shoji, *7th International Conference on μTAS*, 2003, 1275.
26 T. Yasuda, K. Suzuki and I. Shimoyama, *7th International Conference on μTAS*, 2003, 1129.
27 Y. C. Tan, V. Cristini and A. P. Lee, *7th International Conference on μTAS*, 2003, 963.
28 T. Thorsen, W. R. Robert, F. H. Arnold and S. R. Quake, *Phys. Rev. Lett.*, 2001, **86**(18), 4163.
29 T. Nisisako, T. Torii and T. Higuchi, *Lab Chip*, 2002, **2**, 24.
30 S. L. Anna, N. Bontoux and H. A. Stone, *Appl. Phys. Lett.*, 2003, **82**(3), 364.
31 J. D. Tice, D. A. Lyon and R. F. Ismagilov, *Anal. Chim. Acta*, 2004, **507**, 73.
32 V. A. Kuz, *J. Appl. Phys.*, 1991, **69**(19), 7034.
33 C. N. Peiss, *J. Appl. Phys.*, 1989, **65**(12), 5235.
34 Y. C. Tan, J. Collins and A. P. Lee, *Technical Digest of the 12th Transducer Conference*, 2003, 28–31.
35 D. R. Link, S. L. Anna, D. A. Weitz and H. A. Stone, *Phys. Rev. Lett.*, 2004, **92**(5), 54503.

36 J. C. McDonald and D. C. Duffy, *Electrophoresis*, 2000, **21**(2), 27.
37 B. J. Briscoe, C. J. Lawrence and W. G. P. Mietus, *Adv. Colloid Interface Sci.*, 1999, **81**, 1–17.
38 S. S. Sadhal, P. S. Ayyaswamy and J. N. Chung, *Transport phenomena with drops and bubbles*; Springer-Verlag: New York, NY, 1997; pp. 311–401.
39 V. Cristini and Y. C. Tan, *Lab Chip*, **4**, DOI: 10.1039/b403226h.
40 V. Cristini, S. Guido and A. Alfani et al., *J. Rheol.*, 2003, **47**(5), 1283.
41 D. J. Wedlock, *Controlled Particle, Droplet and Bubble Formation*, Butterworth-Heinemann Ltd., Jordan Hill, Oxford, 1994, pp. 579–585.
42 Y. C. Fung, *Biomechanics Circulation*, Springer-Verlag, New York, NY, 1996.
43 J. Eggers, J. R. Lister and H. A. Stone, *J. Fluid Mech.*, 1999, **401**, 293.
44 V. S. Nikolayev, D. Beysens and P. Guenoun, *Phys. Rev. Lett.*, 1996, **76**(17), 3144.